Quark-hadron duality and truncated moments of nucleon structure functions

A. Psaker,[1,2,3] W. Melnitchouk,[1] M. E. Christy,[2] and C. Keppel[1,2]
[1]*Jefferson Laboratory, Newport News, Virginia 23606, USA*
[2]*Hampton University, Hampton, Virginia 23668, USA*
[3]*American University of Nigeria, Yola, Nigeria*
(Received 16 March 2008; published 7 August 2008)

We employ a novel new approach to study local quark-hadron duality using "truncated" moments, or integrals of structure functions over restricted regions of x, to determine the degree to which individual resonance regions are dominated by leading twist. Because truncated moments obey the same Q^2 evolution equations as the leading twist parton distributions, this approach makes possible for the first time a description of resonance region data and the phenomenon of quark-hadron duality directly from QCD.

DOI: 10.1103/PhysRevC.78.025206 PACS number(s): 25.30.Bf, 13.40.Gp, 14.20.Dh, 24.85.+p

I. INTRODUCTION

The structure and interactions of hadrons at intermediate energies represents one of the most outstanding problems in the standard model of particle and nuclear physics. Many hadronic observables can be described at low energies in terms of effective, hadronic (meson and baryon) degrees of freedom, while at high energies perturbative QCD has proved a highly successful approach to describing phenomena in terms of elementary quark and gluon constituents. The precise nature of the transition between the two regimes has remained shrouded in mystery, however, and represents a fundamental challenge to our understanding of strong nuclear interactions within QCD.

One of the most intriguing connections between the low and high energy realms is the phenomenon of quark-hadron duality, in which one finds in certain cases dual descriptions of observables in terms of either explicit quark degrees of freedom, or as averages over hadronic variables. A spectacular example of such a duality is in inclusive electron-nucleon scattering. First observed by Bloom and Gilman in the early days of deep inelastic scattering (DIS) measurements [1], this duality manifests itself in the similarity of structure functions averaged over the resonance region (which is characterized by hadronic bound states) and the scaling or leading twist function describing the high energy, deep inelastic continuum (characterized by scattering from free quarks) [2].

Unraveling the origin of the "Bloom-Gilman" duality from first principles has proved to be a major challenge in QCD. Until now the only rigorous connection with the fundamental theory has been within the operator product or "twist" expansion, in which moments of structure functions are expanded as a series in inverse powers of the virtuality Q^2 of the exchanged photon. The leading, $\mathcal{O}(1)$ term is given by matrix elements of (leading twist) quark-gluon bilocal operators, and is associated with free quark scattering, while the $\mathcal{O}(1/Q^2)$ and higher terms correspond to nonperturbative (higher twist) quark-gluon interactions. Bloom-Gilman duality is then interpreted in this language as the suppression of higher twist contributions to the moments [3].

Recent experimental data [4] suggest that not only moments, but structure functions in individual resonance regions, such as the Δ, S_{11} or F_{15} regions, closely resemble the leading twist structure functions over the same intervals. This indicates that duality also exists locally, in restricted regions of hadronic final state mass W. The appearance of this *local* duality cannot, however, be explained with the theoretical tools presently at our disposal, and insight into the workings of duality for individual resonance regions has been confined to QCD-inspired models of the nucleon. As such our understanding of quark-hadron duality in nucleon structure functions within QCD is incomplete.

In this paper we present a new approach to the study of local quark-hadron duality within a perturbative QCD context, using "truncated" moments of structure functions. The virtue of truncated moments is that they obey a similar set of Q^2 evolution equations as those for parton distributions [5,6], which therefore enables a rigorous connection to be made between local duality and QCD. It allows us to quantify for the first time the higher twist content of various resonance regions, and determine the degree to which individual resonances are dominated by leading twist.

Truncated moments were introduced several years ago by Forte *et al*. [5] to study structure function moments for which small-x data were not available. By restricting or truncating the integration region to some minimum value of the Bjorken x variable, one could avoid the problem of extrapolating parton distributions into unmeasured regions at small x. Later Kotlorz and Kotlorz [6] developed an alternative formulation of the evolution equations which avoids the problem of mixing of higher truncated moments when evolving in Q^2.

In this work we partially follow the latter approach and apply it to the study of structure functions in the *large-x* region, populated by nucleon resonances. In particular, we study the Q^2 evolution of structure functions integrated over specific nucleon resonance regions. To facilitate such an analysis requires extension of the definition of the truncated moments to include both upper and lower truncations. We show that these "doubly truncated" moments also obey the same Q^2 evolution equations. Using recent high-precision data on the proton F_2 structure function from Jefferson Lab and elsewhere, we quantify the size of the higher twists for the lowest three moments in various regions of W. This represents the first quantitative test of local duality in structure functions within a QCD framework.

This paper is organized as follows. In Sec. II we review the essential elements of Q^2 evolution via the DGLAP equations, and introduce truncated moments together with their evolution. We test the accuracy of our numerical evolution procedure in Sec. III, and further study recent proton structure function data in the nucleon resonance region at $W < 2$ GeV. We divide the data into the three traditional resonance regions and extract the leading and higher twist content of each region. Finally, in Sec. IV we summarize the conclusions of this analysis and outline future work.

II. TRUNCATED MOMENTS AND EVOLUTION

A. QCD evolution equations

The Q^2 dependence of a parton distribution function (PDF) $q(x, Q^2)$ is described in perturbative QCD (pQCD) by the DGLAP evolution equations [7]:

$$\frac{dq(x, Q^2)}{dt} = \frac{\alpha_S(Q^2)}{2\pi}(P \otimes q)(x, Q^2), \tag{1}$$

where $t \equiv \ln(Q^2/\Lambda^2_{\rm QCD})$, with $\Lambda_{\rm QCD}$ the QCD scale parameter, and the symbol $\otimes$ denotes the Mellin convolution,

$$(P \otimes q)(x, Q^2) = \int_x^1 \frac{dy}{y}\, P\left(\frac{x}{y}, \alpha_S(Q^2)\right) q(y, Q^2), \tag{2}$$

between the parton distribution q and the splitting function (or the evolution kernel) P. In pQCD the latter can be expanded as a series in the strong running coupling constant $\alpha_S(Q^2)$. For the nonsinglet (NS) case, q is one of the flavor nonsinglet combinations of quark distributions and P the corresponding NS splitting function. For the singlet case, on the other hand, q is a vector whose components are the flavor singlet combination of quark distributions and the gluon distribution, and correspondingly P is a 2×2 matrix of splitting functions.

Taking moments, the convolution in Eq. (1) turns into an ordinary product, and the evolution equations become ordinary first order differential equations in moment space n,

$$\frac{d\mathcal{M}_n(Q^2)}{dt} = \frac{\alpha_S(Q^2)}{2\pi}\,\gamma_n(Q^2)\mathcal{M}_n(Q^2), \tag{3}$$

which can be solved analytically. Here the nth full moment of the parton distribution is defined as

$$\mathcal{M}_n(Q^2) = \int_0^1 dx\, x^{n-1} q(x, Q^2), \tag{4}$$

and the anomalous dimension,

$$\gamma_n(Q^2) = \int_0^1 dz\, z^{n-1} P(z, \alpha_S(Q^2)), \tag{5}$$

is the moment of the splitting function $P(z, \alpha_S(Q^2))$. The PDF can then be determined via the inverse Mellin transform,

$$q(x, Q^2) = \frac{1}{2\pi i}\int_{c-i\infty}^{c+i\infty} dn\, x^{-n}\, \mathcal{M}_n(Q^2). \tag{6}$$

From the definition in Eq. (4), the full moments are obtained by integrating the PDF over all values of the Bjorken variable, $0 \leqslant x \leqslant 1$. Since x is related to the invariant mass squared W^2 of the virtual photon-hadron system, $W^2 = M^2 + Q^2(1-x)/x$, where M is the nucleon mass, to reach the $x \to 0$ limit requires infinite energy; hence in practice some extrapolation to $x = 0$ is always needed to evaluate the moment. Similarly, at finite Q^2 one usually excludes from leading twist analyses the $W < 2$ GeV region in order to avoid low-W nucleon resonances, so an analogous extrapolation to $x = 1$ is also performed.

B. Truncated moments

An alternative approach, which avoids uncertainties from unmeasured regions at low and high x, makes use of the so-called "truncated moments" [5]. In analogy with the full moments, the truncated moments of a PDF $q(x, Q^2)$ are defined as

$$\mathcal{M}_n(x_0, 1, Q^2) = \int_{x_0}^1 dx\, x^{n-1} q(x, Q^2), \tag{7}$$

where the integration is restricted to $x_0 \leqslant x \leqslant 1$ (the first two arguments in $\mathcal{M}_n$ denote the lower and upper limits of the integration). From the evolution equation (1), one can verify that the truncated moments satisfy

$$\frac{d\mathcal{M}_n(x_0, 1, Q^2)}{dt} = \frac{\alpha_S(Q^2)}{2\pi}\int_{x_0}^1 dy\, y^{n-1} q(y, Q^2) \times G_n\left(\frac{x_0}{y}, Q^2\right), \tag{8}$$

where

$$G_n(x, Q^2) = \int_x^1 dz\, z^{n-1} P(z, \alpha_S(Q^2)) \tag{9}$$

is the truncated anomalous dimension. For $x_0 = 0$, the latter reduces to the usual x-independent anomalous dimension, $G_n(0, Q^2) = \gamma_n(Q^2)$, which can be taken outside the integral in Eq. (8). The right hand side then depends only on the nth moment, and the full moments of PDFs evolve independently of each other.

For nonzero x_0, the residual y dependence in the truncated anomalous dimension leads to evolutions equations which are not diagonal in n. This can be seen by expanding $G_n(x_0/y, Q^2)$ as a Taylor series around $y = 1$, and truncating the expansion at a finite order m. Accordingly, Eq. (8) then turns into a system of coupled evolution equations:

$$\frac{d\mathcal{M}_n(x_0, 1, Q^2)}{dt} = \frac{\alpha_S(Q^2)}{2\pi}\sum_{k=0}^{m} c^{(m)}_{n,k}(x_0)\mathcal{M}_{n+k}(x_0, 1, Q^2), \tag{10}$$

where

$$c^{(m)}_{n,k}(x_0) = \sum_{p=k}^{m} \frac{(-1)^{p+k} g^n_p(x_0)}{k!(p-k)!} \quad \text{and}$$
$$g^n_p(x_0) \equiv \frac{\partial^p}{\partial y^p} G_n\left(\frac{x_0}{y}, Q^2\right)\Big|_{y=1}. \tag{11}$$

Unlike the full moments, the evolution of the truncated moment of order n is determined by all truncated moments of

order $n + k$, with $k > 0$. However, the series of couplings to higher moments converges, and can be truncated to any desired accuracy. One can solve Eq. (10) to arbitrarily high accuracy by using a sufficiently large basis of truncated moments. For example, the higher moments ($n \geqslant 2$) can be calculated with excellent accuracy even for a small ($m = 4$) number of terms in the expansion of the truncated anomalous dimension. The first moment, on the other hand, is more sensitive to the truncation point x_0 and the convergence of the truncated anomalous dimension for $n = 1$ is weaker than for the higher moments.

C. Diagonal formulation of truncated moments

The evolution equations satisfied by the truncated moments can be formulated in an alternative way which avoids the problem of mixing of lower moments with higher moments [6]. Inverting the order of integration on the right hand side of Eq. (8) and introducing a new variable $u = x_0(y/x)$, the integral can be written as

$$\int_{x_0}^{1} dx\ x^{n-1}(P \otimes q)(x, Q^2) = (P'_n \otimes \mathcal{M}_n)(x_0, Q^2), \quad (12)$$

with

$$P'_n(z, \alpha_S(Q^2)) = z^n P(z, \alpha_S(Q^2)). \quad (13)$$

The evolution equation for the truncated moments then becomes

$$\frac{d\mathcal{M}_n(x_0, 1, Q^2)}{dt} = \frac{\alpha_S(Q^2)}{2\pi}(P'_n \otimes \mathcal{M}_n)(x_0, Q^2), \quad (14)$$

which is very similar to the original evolution equation (1) for the PDFs. Here P'_n plays the role of the splitting function for the truncated moments. The truncated moments therefore satisfy DGLAP evolution with a modified splitting function $P(z, \alpha_S(Q^2)) \to z^n P(z, \alpha_S(Q^2))$ in the Mellin convolution. The advantage of this approach is that it can be successfully applied to any nth moment and for every truncation point $0 < x_0 < 1$, without the complication of mixing with higher moments.

The evolution equations for the truncated moments can also be generalized to any subset in the x-region, $x_{\min} \leqslant x \leqslant x_{\max}$. Writing the "doubly-truncated" moment of the PDF as

$$\mathcal{M}_n(x_{\min}, x_{\max}, Q^2) = \int_{x_{\min}}^{x_{\max}} dx\ x^{n-1} q(x, Q^2), \quad (15)$$

its Q^2 evolution can be obtained by subtracting the solutions of truncated moments at the points $x_{\min}$ and $x_{\max}$:

$$\mathcal{M}_n(x_{\min}, x_{\max}, Q^2) = \mathcal{M}_n(x_{\min}, 1, Q^2) - \mathcal{M}_n(x_{\max}, 1, Q^2), \quad (16)$$

where $\mathcal{M}_n(x_{\min}, 1, Q^2)$ and $\mathcal{M}_n(x_{\max}, 1, Q^2)$ both satisfy Eq. (14).

III. DATA ANALYSIS

The central aim of this study is to determine the extent to which nucleon structure function data in specific regions in x (or W) are dominated by leading twist. This can be done by constructing empirical truncated moments and evolving them to a different Q^2 using one of two methods. Namely, (i) the structure functions are evolved and the corresponding truncated moments the calculated, or (ii) the moments are evolved directly using the evolution equations in Eq. (14) above. We found the results of both methods to be essentially equivalent. In the study of the proton structure function data there is, however, difficulty in applying the target mass corrections (TMCs) using the latter method. Here in principle one can derive and solve the evolution equations for the target mass corrected moments (the so-called truncated Nachtmann moments), which contain the TMCs explicitly. In practice, to avoid this problem we shall utilize method (i): we evolve the structure functions, correct them for TMCs, and finally calculate their moments.

Deviations of the evolved moments, computed to next-to-leading order (NLO) accuracy, from the experimental data at the new Q^2 then reveal any higher twist contributions in the original data. In particular, we will analyze recent data on the proton F_2^p structure function from Jefferson Lab covering a range in Q^2 from $\lesssim$1 GeV^2 to $\approx$6 GeV^2.

The evolution of the measured truncated moments requires the structure function to be decomposed into its nonsinglet and singlet components. Without performing a global pQCD analysis of the structure function data, it is *a priori* unknown which parts of the structure function are singlet and nonsinglet. To proceed, we shall assume that in our region of interest, at moderate to large x, the proton structure function is well approximated by its nonsinglet component, and will evolve the truncated moments as nonsinglets. The accuracy of this approximation will improve with increasing order of the truncated moments.

A. Evolution of truncated moments

We test the accuracy of the nonsinglet evolution by first evolving a trial structure function whose decomposition into its nonsinglet and singlet components is known. The trial function is evolved exactly, with its nonsinglet and singlet components computed separately, and also evolved under the assumption that the total function can be treated as a nonsinglet. A comparison of the discrepancy between the two evolved truncated moments can then reveal the accuracy of the nonsinglet evolution of the various moments as a function of the truncation region.

There are many methods to solve the Q^2 evolution equations for the truncated moments [8]. The simplest and most direct is to solve the equations by brute force using a suitable numerical integration routine. In this work we use the method of Ref. [9] for the evolution.

To illustrate the method of direct moment evolution, we consider the evolution of the nonsinglet truncated moment, $\mathcal{M}_n^{\rm NS}$, to leading order in α_S (although in practice our numerical results are performed at NLO):

$$\frac{d\mathcal{M}_n^{\rm NS}(x, 1, \tau)}{d\tau} = \int_x^1 \frac{dy}{y} \left(\frac{x}{y}\right)^n P_{\rm NS}^{(0)}\left(\frac{x}{y}\right) \mathcal{M}_n^{\rm NS}(y, 1, \tau), \quad (17)$$

where the leading order NS splitting function is

$$P_{\rm NS}^{(0)}(z) = \frac{4}{3}\left[\frac{1+z^2}{(1-z)_+} + \frac{3}{2}\delta(1-z)\right], \tag{18}$$

and instead of t we use the variable τ, where

$$\tau \equiv -\frac{2}{\beta_0}\ln\left[\frac{\alpha_S(Q^2)}{\alpha_S(Q_0^2)}\right], \tag{19}$$

with $\alpha_S(Q^2) = 4\pi/[\beta_0 \ln(Q^2/\Lambda^2_{\rm QCD})]$ the running coupling constant at leading order, and $\beta_0 = 11 - 2N_f/3$ for N_f quark flavors. By dividing the variables τ and x into small steps, the evolution from τ_j to τ_{j+1} can be written as

$$\mathcal{M}_n^{\rm NS}(x_i, 1, \tau_{j+1}) = \mathcal{M}_n^{\rm NS}(x_i, 1, \tau_j) + \Delta\tau_j \sum_{k=i}^{N_x} \frac{\Delta x_k}{x_k}\left(\frac{x_i}{x_k}\right)^n \times P_{\rm NS}^{(0)}\left(\frac{x_i}{x_k}\right)\mathcal{M}_n^{\rm NS}(x_k, 1, \tau_j), \tag{20}$$

where $\Delta\tau_j = \tau_{j+1} - \tau_j$ and $\Delta x_k = x_k - x_{k-1}$ are the steps at positions j and k, and N_x is the number of steps in x. The final truncated moment at τ_{N_τ} is then obtained by repeating the step in Eq. (20) $(N_\tau - 1)$ times.

For the trial function we take the leading twist proton F_2 structure function computed from the MRST2004 PDF fit [10]. The $n = 2, 4$, and 6 truncated moments of F_2^p are then evolved from $Q^2 = 25$ GeV^2 to 1 GeV^2 using NS evolution, and compared with the exact results using singlet and nonsinglet evolution. The ratios of these are plotted in Fig. 1 as a function of the truncation point $W_{\rm max}$, where $W^2_{\rm max} = M^2 + Q^2(1/x_{\rm min} - 1)$.

Generally the differences between the full and NS evolution are of the order 2–4% for $1.2 \lesssim W_{\rm max} \lesssim 2$ GeV, the traditional nucleon resonance region, and increase with increasing $W_{\rm max}$. Note that at $Q^2 = 1$ GeV^2, $W_{\rm max} = 2$ GeV corresponds to $x_{\rm min} = 0.24$. For the $n = 2$ moment, which is most sensitive to singlet evolution, the differences do not exceed ≈4% for $1.2 \lesssim W_{\rm max} \lesssim 2$ GeV. As expected, for the higher moments the differences are smaller, $\lesssim 2-3\%$ for $n = 4$ and $n = 6$ for $1.3 \lesssim W_{\rm max} \leqslant 2$ GeV. In the region relevant for our study one can therefore safely conclude that the error introduced by evolving the F_2^p moments as nonsinglets is less than 4%. This uncertainty will be included in the errors in our final results.

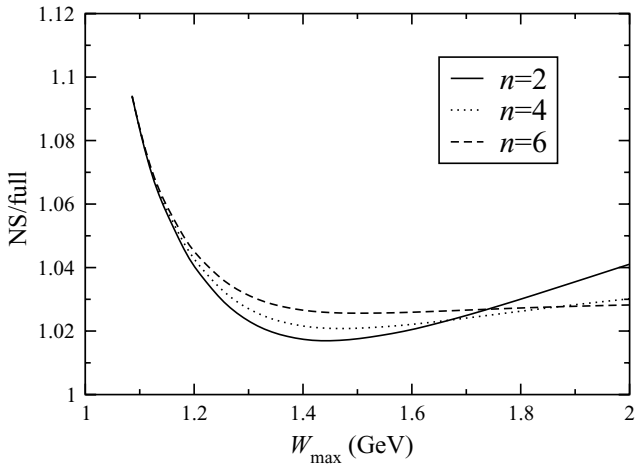

FIG. 1. Ratio of the truncated moments of F_2^p evolved from $Q^2 = 25$ to 1 GeV^2, using NS and full evolution, versus the truncation point $W_{\rm max}$ (or $x_{\rm min}$), for the $n = 2$ (solid), 4 (dotted), and 6 (dashed) moments.

B. Extraction of higher twists

Having tested the accuracy of the nonsinglet evolution we now turn our attention to the analysis of the F_2^p structure function data. In Fig. 2 (top panel) we compare the F_2^p resonance data from Jefferson Lab experiment E91-110 [11] at $Q^2 = 1$ GeV^2 (triangles) with an empirical fit [21] to the data (dashed), and with leading twist fits to the deep-inelastic F_2^p data [20] with (solid) and without (dot-dashed) target mass corrections. The resonance fit [21] describes the F_2^p data to better than 3% over the range $0 \leqslant Q^2 \leqslant 8$ GeV^2 and W^2 from the inelastic threshold up to 10 GeV^2.

Since the data at low Q^2 contain significant contributions arising from kinematical M^2/Q^2 corrections (which, although subleading in Q^2, contribute at leading twist), a direct comparison of data with the leading twist structure function requires the inclusion of TMCs. We do so here by applying the standard TMC prescription for F_2 from Ref. [12] (see also Ref. [13] for a review of TMCs). As is evident from Fig. 2, the leading twist fit to the DIS data, including TMCs, agrees well with the average F_2^p data in each resonance region. A comparison of this fit with the DIS data at $Q^2 = 25$ GeV^2 (bottom panel of Fig. 2) shows the excellent agreement between the leading twist function and the data at this scale.

More specifically, the comparison of the data with the target mass corrected leading twist function illustrates the intriguing phenomenon of Bloom-Gilman duality, where the data in the resonance region oscillate around, and on average are approximately equal to, the leading twist function [1]. This duality reveals itself in the relatively small value of the higher twist contributions at these scales observed in recent high-precision F_2^p measurements—see Ref. [2] for a review of the data. Note that the nonzero value of F_2 with TMCs in the limit $x \to 1$, which is related to the so-called threshold problem, introduces a small additional uncertainty into structure function analyses at low Q^2 [13,14].

To determine the extent to which the F_2^p data at low Q^2 are dominated by leading twist, we assume that the data beyond some large Q^2 value are dominated by twist-2 contributions. In view of the comparison with the data in Fig. 2, in this analysis we take this scale to be $Q^2 = Q_0^2 = 25$ GeV^2. This assumption is also consistent with most global analyses of PDFs, which fit leading twist PDFs to structure function data down to $Q^2 \sim 1$–2 GeV^2 [10,15–17]. Although these analyses typically exclude low-W resonance data, in practice there is little contribution to the low moments from the resonance region $W \leqslant 2$ GeV.

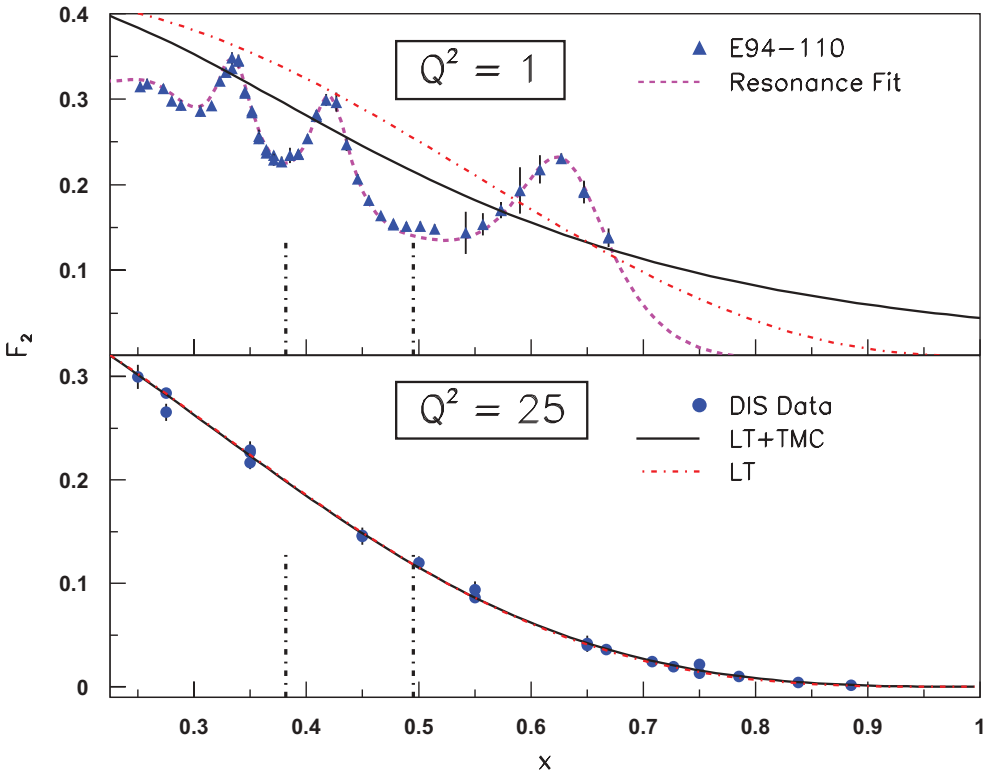

FIG. 2. (Color online) (Top panel) Comparison of proton F_2 data from JLab experiment E91-110 [11] at $Q^2 = 1$ GeV^2 (triangles), and the fit [21] to the data ("Resonance Fit", dashed), with a global fit of DIS data used to extract target mass contributions [20]. Shown is the leading twist DIS fit with ("LT+TMC", solid) and without ("LT", dot-dashed) the TMCs. The vertical lines indicate the extent of the second (S_{11}) resonance region. (Bottom panel) DIS data at $Q^2 = 25$ GeV^2 (circles) compared with the LT and LT+TMC fits.

The analysis method then proceeds in four main steps:

(i) For each W^2 region of interest, the x range to be covered (Δx) is calculated at the particular (lower) Q^2 where the leading twist contribution is to be extracted. For the second (S_{11}) resonance region, for example, this is indicated by the vertical lines in Fig. 2 (top panel).

(ii) The structure function extracted from a precision fit to data [20] at the starting scale $Q_0^2 = 25$ GeV^2 is evolved in leading twist down to lower Q^2 and the TMCs are applied. Note that at the higher Q_0^2 value the same interval Δx is used, as, e.g., indicated by the vertical lines in Fig. 2 (bottom panel), which corresponds to a higher W range.

(iii) The truncated moment of the evolved leading twist, target mass corrected structure function from Step 2 is calculated for the interval Δx defined in Step 1.

(iv) The truncated moment of the resonance data at Q^2 is calculated in the interval Δx and compared with the result of Step 3.

After evolving down to $Q^2 = 1$ GeV^2 and applying the target mass corrections, the $n = 2$ truncated moment $\mathcal{M}_2$ is shown in Fig. 3(a) as a function of $W_{\rm max}$, where it is compared with the moment of the actual data at $Q^2 = 1$ GeV^2. The difference between the evolved curve and the data attests to the presence of higher twist contributions in the data at $Q^2 = 1$ GeV^2. The importance of the TMCs is also clearly evident, and these in fact reduce the difference between the leading twist moment and the data by some 40% for large $W_{\rm max}$. The ratio of the truncated moments of the data to the leading twist in Fig. 3(b) illustrates that without TMCs the leading twist moment differs from the data by ∼20% for $W_{\rm max} > 1.5$ GeV. After correcting for TMCs, the size of the apparent higher twists is reduced to ∼15%. It is imperative, therefore, that the kinematical effects associated with finite values of Q^2/ν^2 be properly accounted for before drawing any conclusions about higher twists from data.

Note that the truncated moments displayed in Fig. 3 are computed over the range $W_{\rm th} \leqslant W \leqslant W_{\rm max}$, where the $W_{\rm th} = M + m_\pi$ is the inelastic threshold. This is consistent with the assumption that the truncated moments at $Q_0^2 = 25$ GeV^2 are entirely of twist-2, since the elastic cross section contributes only to the higher twist part of the structure function. For a meaningful comparison, we therefore do not include the elastic contribution at lower Q^2. At $Q^2 = 1$ GeV^2 this corresponds to the integration range $x_{\rm min} \leqslant x \leqslant x_{\rm th}$, where $x_{\rm th} = [1 + m_\pi(m_\pi + 2M)/Q^2]^{-1} \simeq 0.78$.

The results in Fig. 3 give a clear indication of the magnitude and sign of higher twists in the data at $Q^2 = 1$ GeV^2. To quantify the higher twist content of the specific resonance regions, and at different values of Q^2, we consider several intervals in W : $W_{\rm th}^2 \leqslant W^2 \leqslant 1.9$ GeV^2, corresponding to the traditional $\Delta(1232)$ (or first) resonance region; $1.9 \leqslant W^2 \leqslant 2.5$ GeV^2 for the $S_{11}(1535)$ (or second) resonance region; and

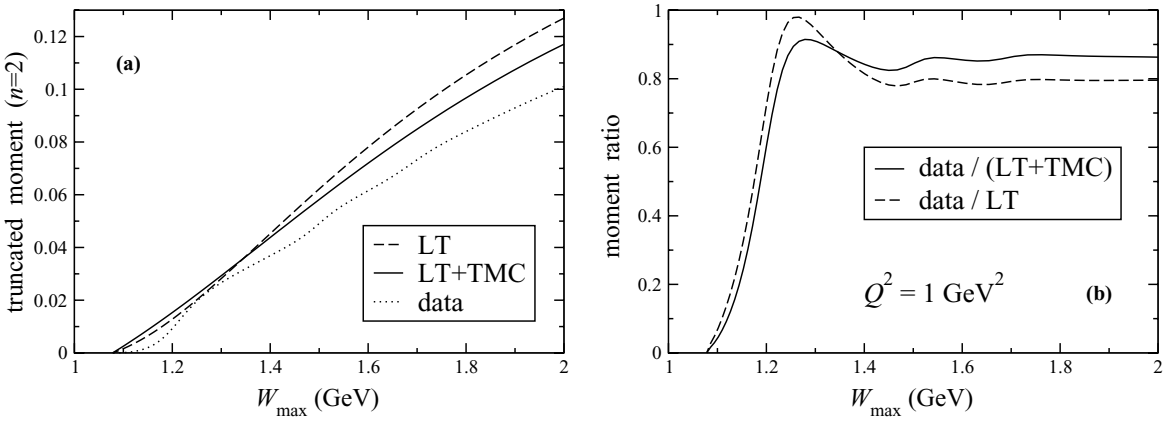

FIG. 3. (a) Truncated moment $\mathcal{M}_2$ as a function of the truncation point $W_{\rm max}$ at $Q^2 = 1$ GeV^2, evolved as leading twist (LT) from $Q_0^2 = 25$ GeV^2 with (solid) and without (dashed) target mass corrections (TMC), and compared with the moment calculated from data (dotted) at $Q^2 = 1$ GeV^2. (b) Ratio of the $\mathcal{M}_2$ truncated moments of the data to the leading twist + TMC (solid), and data to leading twist without TMC (dashed) at $Q^2 = 1$ GeV^2.

$2.5 \leqslant W^2 \leqslant 3.1$ GeV^2 for the $F_{15}(1680)$ (or third) resonance region. The $n = 2$ truncated moments corresponding to these regions are plotted in Fig. 4 for various Q^2 values, from $Q^2 = 1$ GeV^2 to $Q^2 = 6$ GeV^2. Shown are ratios of moments calculated from the data to the moments obtained from NLO evolution of the leading twist moments from $Q_0^2 = 25$ GeV^2, corrected for target mass effects. Below $Q^2 = 1$ GeV^2 the applicability of a pQCD analysis becomes doubtful and the decomposition into leading and higher twists is no longer reliable.

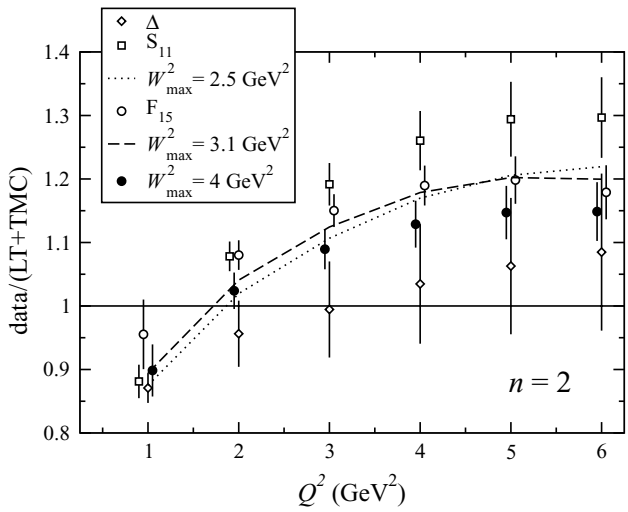

FIG. 4. Q^2 dependence of the ratio of $n = 2$ truncated moments $\mathcal{M}_2$ calculated from the data and from leading twist evolution from $Q_0^2 = 25$ GeV^2 (including TMCs), for various intervals in W: the first (Δ) resonance region (diamonds), second (S_{11}) resonance region (squares), the first and second combined, corresponding to $W^2_{\rm max} = 2.5$ GeV^2 (dotted curve), third (F_{15}) resonance region (open circles), first three regions combined, $W^2_{\rm max} = 3.1$ GeV^2 (dashed curve), and the entire resonance region $W^2_{\rm max} = 4$ GeV^2 (filled circles). Note that some of the points are offset slightly for clarity.

The results indicate deviations from leading twist behavior of the entire resonance region data (filled circles in Fig. 4) at the level of $\lesssim$15% for all values of Q^2 considered, with significant Q^2 dependence for $Q^2 \lesssim 4$ GeV^2. This is made more explicit in Fig. 5, where the higher twist contributions to $\mathcal{M}_2$ (defined as the difference between the total and leading twist moments) are shown as ratios of the moments evaluated from the data.

The strong Q^2 dependence of the higher twists is evident here in the change of sign around $Q^2 = 2$ GeV^2, with the higher twists going from $\approx -10\%$ at $Q^2 = 1$ GeV^2 to $\approx$10–15% for $Q^2 \approx 5$ GeV^2. The slope at $Q^2 \approx$ 1–2 GeV^2 would be decreased if the full NS + singlet evolution were performed, as evident from Fig. 1, since the NS-only evolution leads to a few percent overestimate of the LT+TMC results. At larger Q^2 the higher twists are naturally expected to decrease, once the leading twist component of the moments begins to

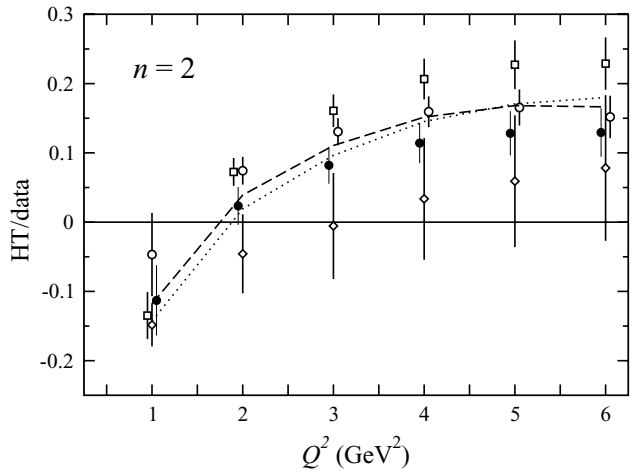

FIG. 5. Q^2 dependence of the fractional higher twist (HT) contribution to the $n = 2$ truncated moment data, for various intervals in W (as in Fig. 4).

dominate. Note that the extraction of higher twists beyond $Q^2 = 6$ GeV^2 would require evolution from a starting scale larger than the $Q_0^2 = 25$ GeV^2 used in this analysis. At larger Q^2, however, data in the large-x region, which determines the behavior of the resonances after evolution to lower Q^2, are not well determined, making extraction of higher twists beyond $Q^2 \approx 6$ GeV^2 problematic at present.

Turning to the individual resonance regions, the results in Figs. 4 and 5 show that in the Δ region (diamonds) the higher twist contributions are smallest in magnitude at large Q^2, decreasing from $\approx -15\%$ of the data at $Q^2 = 1$ GeV^2 to values consistent with zero (within errors) at larger Q^2. The higher twists are largest, on the other hand, for the S_{11} region (squares), where they vary between $\approx -15\%$ of the data at $Q^2 = 1$ GeV^2 and 20–25% at $Q^2 \sim 5$ GeV^2. Combined, the higher twist contribution from the first two resonance regions (dotted curve) is $\lesssim$15% in magnitude for all Q^2. The rather dramatic difference between the Δ and the S_{11}, may, at least in part, be due to the choice of the differentiation point of $W^2 = 1.9$ GeV^2. A lower W^2 choice, for instance, would lower the higher twist content of the S_{11} at large Q^2, while raising that of the Δ. However, our W^2 choice corresponds to the local minimum between these two resonances in the inclusive spectra, and is the one most widely utilized.

The higher twist content of the F_{15} region (open circles) is similar to the S_{11} at low Q^2, but decreases more rapidly for $Q^2 > 3$ GeV^2. The higher twist content of the first three resonance regions combined (dashed curve) is $\lesssim$15–20% in magnitude for $Q^2 \leqslant 6$ GeV^2. Integrating up to $W^2_{\rm max} = 4$ GeV^2 (filled circles), the data on the $n = 2$ truncated moment are found to be leading twist dominated at the level of 85–90% over the entire Q^2 range.

The results in Figs. 4 and 5 contain two sources of uncertainty: from the experimental uncertainty on the F_2 data (statistical and systematic), and from the nonsinglet evolution of the data. For the experimental error we take an overall uncertainty of 2% for all truncated moment data, with the exception of the $n = 4$ and $n = 6$ moments for $W^2_{\rm max} = 1.9$ and 4 GeV^2, where the experimental uncertainties are 4% and 3% for $\mathcal{M}_4$, and 5% and 4.5% for $\mathcal{M}_6$ for the two W regions, respectively. The evolution error is estimated by comparing the nonsinglet evolution with the full evolution using the MRST fit, as in Fig. 1, with the appropriate correction factor applied at each Q^2 and W interval. We do not assign an uncertainty for the structure function at the $Q_0^2 = 25$ GeV^2 input scale, as this is negligible for all but the Δ region analysis at $Q^2 = 6$ GeV^2, where we estimate it to be $\lesssim$3%.

Note that the size of the error bars on the S_{11} and F_{15} data points at the lowest Q^2 are larger than those for the Δ. This is due to the fact that these resonances lie at higher W, and hence at lower values of x compared to the Δ, and where the NS approximation to the full evolution is not as good as at large x. The error bar on the Δ is smaller at the same low Q^2 values since it appears at larger x, where the NS versus full evolution differences are smaller.

The relatively small size of the higher twists at scales $\sim$ few GeV^2 is consistent with the qualitative observations made in earlier data analyses about the approximate validity of Bloom-Gilman duality [4]. In this analysis we are able to for the first time quantify precisely the degree to which this duality holds as a function of Q^2 (see also Ref. [18]). The fact that duality works better (higher twists are smaller) when more resonances are included is also borne out in various quark model studies [2,19].

Similar behavior is found also for the $n = 4$ and $n = 6$ truncated moment ratios, illustrated in Figs. 6 and 7, respectively. For the higher moments, the overall magnitude of the higher twists is qualitatively similar to the $n = 2$ moments, although the Q^2 values at which they start decreasing in importance are larger. At low Q^2 values the higher twist contributions are also relatively larger for higher moments: at $Q^2 = 1$ GeV^2, for example, the magnitude of the higher twist component of the $W^2 < 4$ GeV^2 region increases from $\sim$10% for the $n = 2$ moment, to $\sim$15–20% for $n = 4$, and $\sim$20–30% for $n = 6$. This behavior can be understood from the relatively

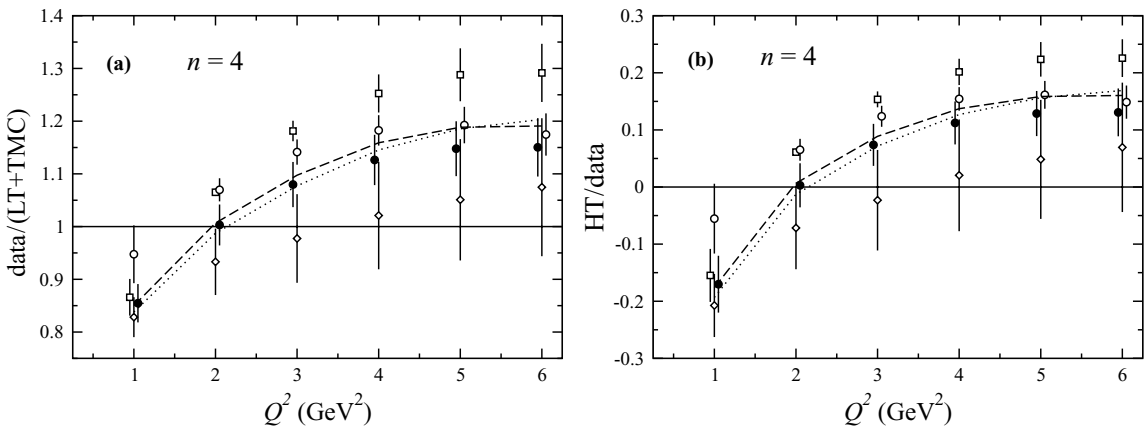

FIG. 6. (a) Q^2 dependence of the ratio of truncated moments $\mathcal{M}_4$ calculated from the data and from leading twist evolution from $Q_0^2 = 25$ GeV^2 (including TMCs), for various intervals in W (labels as in Fig. 4). (b) Fractional higher twist contribution to the $n = 4$ truncated moment data, for various intervals in W (as in Fig. 5).

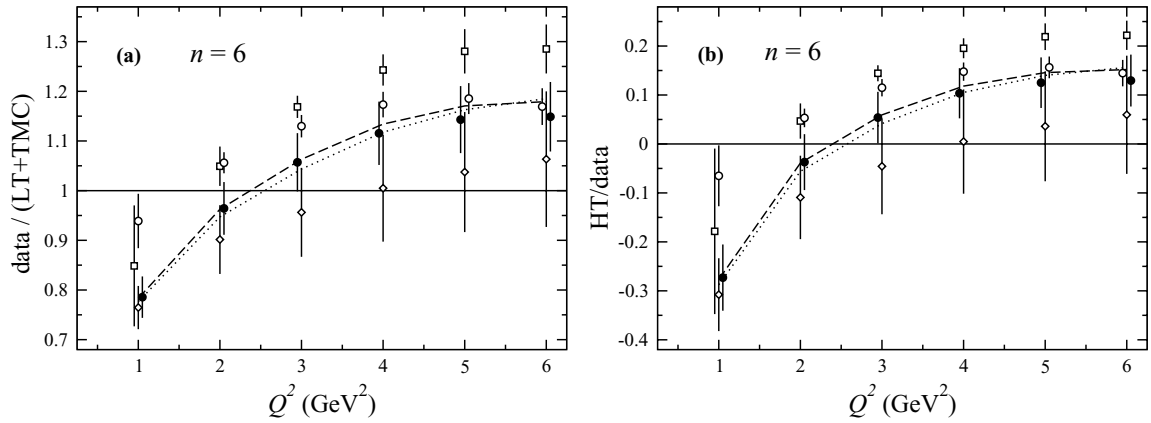

FIG. 7. (a) Ratio of truncated moments $\mathcal{M}_6$ calculated from the data and from leading twist evolution from $Q_0^2 = 25$ GeV^2 (including TMCs), for various intervals in W (labels as in Fig. 4). (b) Fractional higher twist contribution to the $n = 6$ truncated moment data, for various intervals in W (as in Fig. 5).

greater role played by the nucleon resonances and the large-x region, which is emphasized more by the (x-weighted) higher moments.

IV. CONCLUSION

Quark-hadron duality in nucleon structure functions remains an intriguing empirical phenomenon which challenges our understanding of strong interaction dynamics, as one transitions from hadronic degrees of freedom in the nucleon resonance region to quarks and gluons in the deep inelastic continuum. Until now the only rigorous connection with QCD has been for moments of structure functions analyzed within the twist expansion. Any insight about the workings of duality for individual resonances, or specific resonance regions, has been confined to QCD-inspired models of the nucleon.

In this paper we have presented a new approach to the study of local quark-hadron duality within a perturbative QCD context, using so-called *truncated* moments of structure functions. The fact that truncated moments obey a similar set of Q^2 evolution equations to the DGLAP equations for parton distributions enables a rigorous connection to be made between local quark-hadron duality and QCD. It allows us to quantify for the first time the higher twist content of various resonance regions, and determine the degree to which individual resonance regions are dominated by leading twist.

We find deviations from leading twist behavior of the truncated moments of the resonance region data ($W \leqslant 2$ GeV) at the level of $\lesssim$15% for $Q^2 > 1$ GeV^2. Significant Q^2 dependence in the ratio of moments of data to leading twist is evident for $Q^2 \lesssim 3$ GeV^2, with the higher twists changing sign around $Q^2 = 2$ GeV^2. For the $n = 2$ truncated moment, $\mathcal{M}_2$, the higher twists are found to vary from $\approx -10\%$ at $Q^2 = 1$ GeV^2 to $\approx$10–15% at $Q^2 \approx 5$ GeV^2.

Separating the $W \leqslant 2$ GeV data into the three traditional resonance regions, our results indicate that at a scale of $Q^2 = 1$ GeV^2 the Δ resonance region contains about -15% higher twist component of the total $\mathcal{M}_2$, but is consistent with zero at larger Q^2. The higher twists in the second (S_{11}) and third (F_{15}) resonance regions are larger in magnitude, with the S_{11} ranging from $\approx -15\%$ at $Q^2 = 1$ GeV^2 to 20–25% at $Q^2 \sim 5$ GeV^2, and the F_{15} varying from 0 and 15% over the same range.

Similar behavior is found also for the $n = 4$ and $n = 6$ truncated moments. Here the relatively greater role played by the resonances due to the large-x enhancement leads to larger higher twists at the same Q^2. At $Q^2 = 1$ GeV^2, for example, the higher twist component of the $W \leqslant 2$ GeV region increases from around -10% for $\mathcal{M}_2$ to $\approx -15\%$ for $\mathcal{M}_4$, and $\approx -25\%$ for $\mathcal{M}_6$.

In contrast to earlier analyses of duality using complete moments of structure functions which have quantified the total higher twist content over all x, this analysis in terms of truncated moments reveals the distribution of higher twist corrections over various regions in x (or W). Note that, unlike many previous moment analyses, an effort was also made to quantify the uncertainty associated with evolving the structure function data as a nonsinglet, which was found to be $\lesssim$4%.

While this analysis has been to some extent exploratory, it has illustrated an encouraging new approach to quantifying and understanding local Bloom-Gilman duality within a well-defined theoretical framework. It opens the way to further study of local duality in other structure functions, such as the longitudinal structure function F_L or spin-dependent structure functions.

ACKNOWLEDGMENTS

We thank I. Cloët for helpful communications, and S. Kumano for providing the Q^2 evolution code from Ref. [9]. This work was supported by the U.S. Department of Energy contract DE-AC05-06OR23177, under which Jefferson Science Associates, LLC operates the Thomas Jefferson National Accelerator Facility, and National Science Foundation grant 0400332.

[1] E. D. Bloom and F. J. Gilman, Phys. Rev. Lett. **25**, 1140 (1970).
[2] W. Melnitchouk, R. Ent, and C. Keppel, Phys. Rep. **406**, 127 (2005).
[3] A. De Rujula, H. Georgi, and H. D. Politzer, Ann. Phys. (NY) **103**, 315 (1977).
[4] I. Niculescu *et al*., Phys. Rev. Lett. **85**, 1186 (2000).
[5] S. Forte and L. Magnea, Phys. Lett. **B448**, 295 (1999); S. Forte, L. Magnea, A. Piccione, and G. Ridolfi, Nucl. Phys. **B594**, 46 (2001); A. Piccione, Phys. Lett. **B518**, 207 (2001).
[6] D. Kotlorz and A. Kotlorz, Phys. Lett. **B644**, 284 (2007).
[7] V. N. Gribov and L. N. Lipatov, Sov. J. Nucl. Phys. **15**, 438, 675 (1972); Y. L. Dokshitzer, Sov. Phys. JETP **46**, 641 (1977); G. Altarelli and G. Parisi, Nucl. Phys. **B126**, 298 (1977).
[8] T. Weigl and W. Melnitchouk, Nucl. Phys. **B465**, 267 (1996).
[9] M. Miyama and S. Kumano, Comput. Phys. Commun. **94**, 185 (1996); S. Kumano and T. H. Nagai, J. Comput. Phys. **201**, 651 (2004).
[10] A. D. Martin, R. G. Roberts, W. J. Stirling, and R. S. Thorne, Phys. Lett. **B604**, 61 (2004).
[11] Y. Liang *et al*., JLab Experiment E94-110, arXiv:nucl-ex/0410027.
[12] H. Georgi and H. D. Politzer, Phys. Rev. D **14**, 1829 (1976).
[13] I. Schienbein *et al*., J. Phys. G: Nucl. Part. Phys. **35**, 053101 (2008).
[14] F. M. Steffens and W. Melnitchouk, Phys. Rev. C **73**, 055202 (2006).
[15] W. K. Tung, H. L. Lai, A. Belyaev, J. Pumplin, D. Stump, and C. P. Yuan, J. High Energy Phys. 02 (2007) 053.
[16] J. Blumlein, H. Bottcher, and A. Guffanti, Nucl. Phys. **B774**, 182 (2007).
[17] L. Del Debbio, S. Forte, J. I. Latorre, A. Piccione, and J. Rojo, J. High Energy Phys. 03 (2007) 039.
[18] S. Liuti, R. Ent, C. E. Keppel, and I. Niculescu, Phys. Rev. Lett. **89**, 162001 (2002); N. Bianchi, A. Fantoni, and S. Liuti, Phys. Rev. D **69**, 014505 (2004).
[19] F. E. Close and N. Isgur, Phys. Lett. **B509**, 81 (2001); N. Isgur, S. Jeschonnek, W. Melnitchouk, and J. W. Van Orden, Phys. Rev. D **64**, 054005 (2001); F. E. Close and W. Melnitchouk, Phys. Rev. C **68**, 035210 (2003); Q. Zhao and F. E. Close, Phys. Rev. Lett. **91**, 022004 (2003); S. Jeschonnek and J. W. Van Orden, Phys. Rev. D **69**, 054006 (2004).
[20] M. E. Christy *et al*. (to be published).
[21] M. E. Christy and P. E. Bosted, arXiv:0712.3731 [hep-ph].